IOP Conf. Series: Materials Science and Engineering **381** (2018) 012180 doi:10.1088/1757-899X/381/1/012180

Cobalt-free Li-Rich $0.1Li_2MnO_3$•$0.9LiNi_{0.56}Mn_{0.44}O_2$ with High Performances as Cathode Material for Lithium-ion Batteries

Shumei Dou[a,*], Fenyan Wei[b], Huiqin Li[c,*] and Ping Li[d]

Engineering research center of advanced ferroelectric functional materials, Shaanxi Key Laboratory of Phytochemistry, College of Chemistry and Chemical Engineer, Baoji University of Arts and Sciences, Baoji, Shaanxi, China 721013
Email: [a]dsmwxsh@163.com, [b]weifenyan@163.com, [c]snowtrue@126.com, [d]710331585@qq.com

Abstract. The cobalt-free Li-rich layered oxide $0.1Li_2MnO_3$ $0.9LiNi_{0.56}Mn_{0.44}O_2$ is successfully synthesized by a coprecipition method followed by high-temperature calcinations. The compostions and structures of the material have been investigated by X-ray diffraction (XRD), scanning electron microscopy (SEM), X-ray photoelectron spectroscopy (XPS) and the results revealed that the sample possesses typical α-$NaFeO_2$ layered structure with a weak reflection of $LiMnO_6$, and of microspheres with porous surface. Electrochemical measurements showed that the cobalt-free Li-rich sample delivers good cycling stability and rate capability with initial discharge capacity of 263, 173, 137 and 57 mAh g^{-1} at different current density of 50, 160, 320 and 640 mA g^{-1}, respectively. The electrochemical performances of the cobalt-free Li-rich $0.1Li_2MnO_3$ $0.9LiNi_{0.56}Mn_{0.44}O_2$ could be related to not only the synergistic effect of specific morphology and appropriate size but also the porous surface.

1. Introduction

Rechargeable lithium-ion batteries which have been widely used as cathode materials in mobile phones, laptons and other portable electronic devices as well as electric vehicles, energy storage power stations, medical equipments, aerospaces and other fields commercialized have a broad application prospects in the future, because they meet most of the requirements such as high energy and high power density. The demands for the next generation lithium-ion batteries with high-performance have increased in terms of energy density, safety and cost [1]. Among all the available options, adopting cathodes with a higher capacity is one of the most effective approaches for improving the energy density [2, 3]. In this regrad, the composites between Li_2MnO_3 and $LiMO_2$ (M=Mn, Ni, Co, Fe, Cr, etc.) can deliver a high discharge capacity of more than 250 mAh g^{-1} in the voltage range of 2.0-4.8 V and exhibit excellent cycling performances [4-6], which make them ideal candidate cathode materials.

Despite their excellent capacities and high energy densities, these Li-rich materials suffer from some drawbacks including large irreversible capacity losses in the initial cycle, capacity and discharge voltage fading in the subsequent cycles [7, 8]. A lot of efforts have been applied to improve the electrochemical properties of cathode materials such as doping ions [9-14] to stabilize the crystal structure, surface coating [15-18] to suppress the undesired surface side reactions, different morphorlogies and article sizes [19-22] to reduce lithium-ion diffusion length, and so on. However, there is also an irreversible oxygen loss during the 1st charging process that creates microcracks at the cathode surface in the conjunction with lattice distortion, producing a large irreversible capacity fading and subsequent lowering of the cycling performance [23]. In addition, the cost, toxity and safety of

cobalt have prevented the widespread use of cobalt-containing cathode materials. Therefore, in this paper, cobalt-free cathode material Li-rich $0.1Li_2MnO_3 \cdot 0.9LiNi_{0.56}Mn_{0.44}O_2$ have been successfully synthesized by a coprecipition approach followed by high-temperature calcinations. The structures and electrochemical properties were also investigated.

2. Experimental

2.1. Material synthesis

All reagents in the study were of analytical grade and used without further purification. The cobalt-free Li-rich layered oxide $0.1Li_2MnO_3 \cdot 0.9LiNi_{0.56}Mn_{0.44}O_2$ were prepared by a coprecipition method followed by high-temperature calcinations. The specific preparation is as follows: precursor nickel-manganese carbonate was prepared by coprecipitation from aqueous mixture of $NiSO_4 \cdot 6H_2O$, $MnSO_4 \cdot H_2O$ (Ni:Mn = 1:1, molar ratio; the combined concentration was 0.04 mol L^{-1}) and 0.10 mol L^{-1} Na_2CO_3 aqueous solution. The solution was mixed slowly in a nitrogen filled reactor and the pH of the mixed solution was kept in the range of 8~9 at 55 ^oC with continuous stirring during the precipitation process. After filtering, washing and drying at around 100 ^oC under vacuum about 10 h, the as-synthesized precursor particles was collected. To prepare $0.1Li_2MnO_3 \cdot 0.9LiNi_{0.56}Mn_{0.44}O_2$, the obtained $(Mn_{0.5}Ni_{0.5})CO_3$ and Li_2CO_3 were mixed at a molar ratio of 0.58:1 by using a ball mill with absolute ethyl alcohol, and then the mixture was pressed into pellets. The pellets were heated at 500 ^oC for 3 h in air before heating up to 900 ^oC for 15 h and then quenched to room temperature.

2.2. Materials characterization

XRD patterns of the samples were examined with a D/MAX-2500 X-ray diffract meter (made in Japan) using Cu K**α** radiation in the 2 theta range of 10-80^o. The contents of the elements in the synthesized samples were determined by inductively coupled plasma (ICP) that recorded on Thermo Fisher ICAP 6300. The morphology and particle size of the samples were investigated by field emission scanning electron microscopy (SEM) on a JSM-6700F instrument working at 5 KV. The valence states of metal ions were determined by X-ray photoelectron spectroscopy (XPS) performed on an ESCA-LAB MK II apparatus performed with a monochromatic Al Ka X-ray source.

2.3. Electrochemical test

For the preparation of cathode sheets, slurry was formed by mixing the active material, acetylene black, and binder (polyvinylidene fluoride, dissolved in N-methyl-2-pyrrolidone) in a weight ratio of 8:1:1. The slurry was spread uniformly on aluminium foil. The electrodes were dried under vacuum at 120 ℃ for 10 h and then pressed under 60 MPa and weighted. 1 M LiPF6 in a 1:1 ethylene carbonate/diethyl carbonate was used as electrolyte, and lithium foil was used as anode. A thin sheet of microporous polypropylene insulated the positive electrode from negative electrodes. Battery assembly was carried out in an argon-filled glove box. Charge and discharge profiles were collected by galvanostatically cycling between 2.5 and 4.8 V (Shenzhen Neware, BTS, and China). Cycling voltammetry (CV) was carried out on electrochemical workstation (CHI 660C) with a scan range of 2.5-4.8 V (vs.Li/Li^+) at a scan rate of 0.2 mV s^{-1}.

3. Results and discussion

ICP analysis technique was used to determine the average chemical compositions of the as-prepared material, and the results were listed in table 1. The atomic ratios of Li, Ni, and Mn for the sample are normalized by fixing the atomic ratio of Ni: Mn at 1: 1. Based on the results of ICP, it can be found that the measured cation ratios of Li: Ni: Mn is well in agreement to the intended composition, which implies that the metal oxides are homogeneously reacted.

Table 1. Chemical composition (wt. %) of the prepared material determined by ICP.

[Li]	[Ni]	[Mn]	[formula]
[7.86]	[28.46]	[26.43]	$[Li[Li_{0.12}Ni_{0.44}Mn_{0.44}]O_2$ or $0.1Li_2MnO_3 \cdot 0.9LiNi_{0.56}Mn_{0.44}O_2]$

The XRD pattern of the $0.1Li_2MnO_3$ $0.9LiNi_{0.56}Mn_{0.44}O_2$ is revealed in figure 1. All the diffraction peaks of the sample can be well-indexed to **α**-$NaFeO_2$ layered hexagonal structure with the space group of R-3m (No. 166) except the peaks between 20^o and 25^o (2θ), which can be ascribed to the existence of monoclinic Li_2MnO_3 component with space group C/2m, corresponding to the $LiMnO_6$ cation ordering in the transition metal layers of Li_2MnO_3 [24-26]. Meanwhile, the distinct splitting of peak between the adjacent of (006)/(102) and (018)/(110) can be obviously observed, indicating a typical layered structure [27, 28]. In addition, the integrated intensity ratio of I(003)/I(104) and $(I_{(006)}+I_{(012)})/I_{(101)}$ (R factor) can be used to evaluate the layered structure and the degree of cation mixing, and with that the ratio of $I_{(003)}/I_{(104)}$ is higher than 1.2, the R factor is lower than 0.4, the as-prepared materials can be of better layered structrue and lower degree of cation mixing [29, 30]. The intensity ratio of I(003)/I(104) and R factor for the the $0.1Li_2MnO_3$ $0.9LiNi_{0.56}Mn_{0.44}O_2$ were 1.48 and 0.398, respectively, indicating the sample is of a favorable layered structure with few cation mixing.

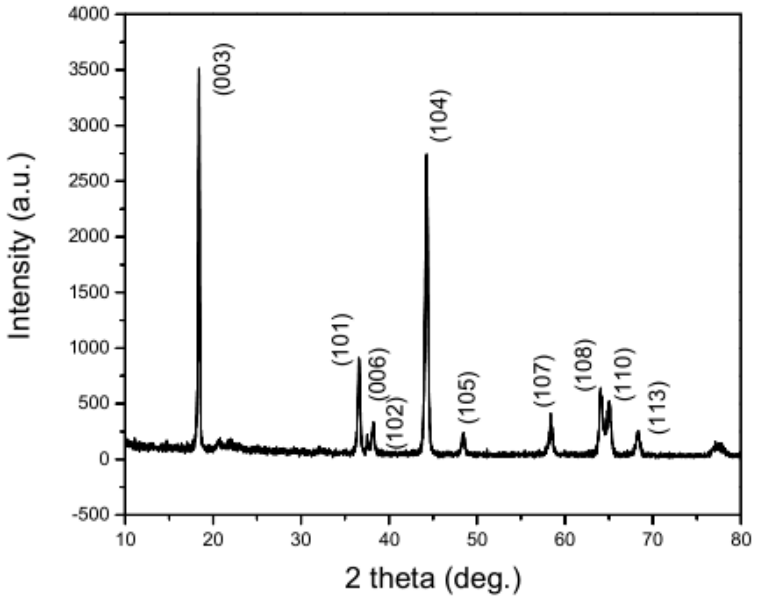

Figure 1. XRD pattern of the cobalt-free Li-rich $0.1Li_2MnO_3$ $0.9LiNi_{0.56}Mn_{0.44}O_2$ material.

Figure 2 shows typical SEM images of $0.1Li_2MnO_3$ $0.9LiNi_{0.56}Mn_{0.44}O_2$. It can be found that $0.1Li_2MnO_3$ $0.9LiNi_{0.56}Mn_{0.44}O_2$ has microspheres with diameter of 4-6 **μ**m from figure 2a. Moreover, the microspheres are comprised of densely aggregated primary grains with sizes of 100-200 nm as shown in figure 2b. The surface of layered oxide $0.1Li_2MnO_3$ $0.9LiNi_{0.56}Mn_{0.44}O_2$ are very rough and there are many small size pores resulted in the emission of CO_2 gas during the calcination process of the precursor $Mn_{0.5}Ni_{0.5}CO_3$ with Li_2CO_3, according to the following equations:

$$2Ni_{0.5}Mn_{0.5}CO_3 + 2O_2 \rightarrow (Ni_{0.5}Mn_{0.5})_2O_3 + 2CO_2$$

$$Li_2CO_3 \rightarrow Li_2O + CO_2$$

$$(Ni_{0.5}Mn_{0.5})_2O_3 + 1.1Li_2O + 0.05O_2 \rightarrow 2\,(0.1Li_2MnO_3\ 0.9LiNi_{0.56}Mn_{0.44}O_2)$$

The inner structure of $0.1Li_2MnO_3$ $0.9LiNi_{0.56}Mn_{0.44}O_2$ microspheres can be demonstrated by section of microspheres. After careful observation, the $0.1Li_2MnO_3$ $0.9LiNi_{0.56}Mn_{0.44}O_2$ microspheres are of microspherical structure with three layers similar to eggs as demostrated in figure 2c. This structure and porous surface can markedly shorten the diffusion distance for lithium ion and enhance the contact areas between cathode material and electrolyte.

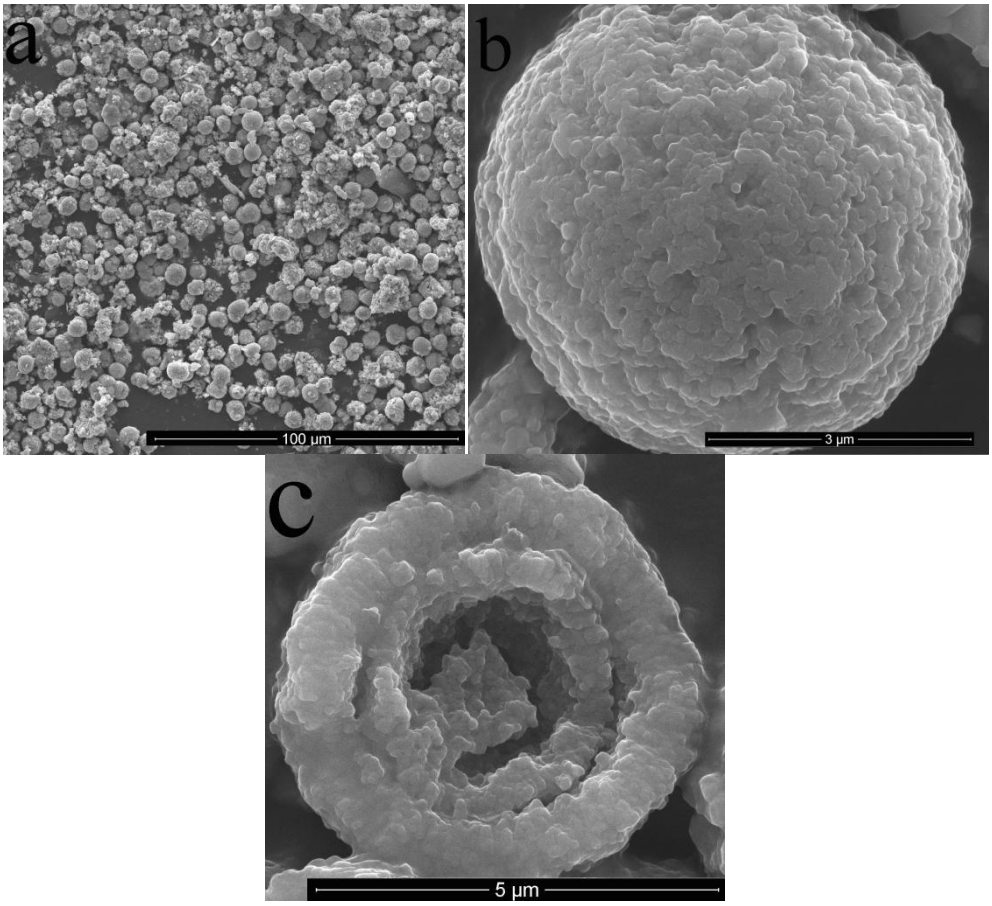

Figure 2. SEM images of the cobalt-free Li-rich $0.1Li_2MnO_3 \cdot 0.9LiNi_{0.56}Mn_{0.44}O_2$ material.

In order to confirm the oxidation states of each transition metal elements (Ni and Mn) for the cobalt-free Li-rich $0.1Li_2MnO_3 \cdot 0.9LiNi_{0.56}Mn_{0.44}O_2$ material, the corresponding XPS spectra of Ni 2p and Mn 2p were carried out as shown in figure 3. It can be observed in figure 3a that the binding energies of Ni $2p_{3/2}$ main pesk, Ni $2p_{3/2}$ satellite peak and Ni $2p_{1/2}$ are 855.3 eV, 861.4 eV, and 872.9 eV, respectively. Among these peaks, the Ni $2p_{3/2}$ satellite peak is characteristic of Ni^{2+}, in accordance with the standard Ni^{2+} in the $LiW_xNi_{0.5}Mn_{1.5-x}O_4$ sample [31]. On the other hand, the binding energy of Ni $2p_{1/2}$ is similar to the Ni^{2+} in the $Li_2MnO_3 \cdot LiMn_{1/3}Ni_{1/3}Co_{1/3}O_2$ [32]. Concerning the Ni $2p_{3/2}$ main peak, it has been previously reported that the binding energy of Ni2+ in Li1.16Ni0.15Co0.19Mn0.50O2 is 854.0 eV [33] and that of Ni^{3+} in $LiNiO_2$ is at 855.5 eV [34]. In this work, the binding energy at 855.3 eV is exactly located in the range of 854.0 and 855.3 eV, indicating the oxidation state of Ni ions consists of mixed +2 and +3 [35]. Additionally, the XPS spectrum of Mn $2p_{3/2}$ shows the characteristic peak at binding energy of 642.5 eV in figure 3b, which is closer to the value measured for Mn^{4+} in -MnO_2 (642.4 eV) than the value measured for Mn^{3+} in $Li_2Mn_2O_4$ (641.1 eV) [36]. Therefore, the valences of the Mn in compounds were considered to be tetravalent without trace of Mn^{3+}. Consequently, the XPS results manifest that the oxidation states of Mn elements in the as-prepared material are principally +4, and that of Ni ions contains +2 and +3 simultaneously.

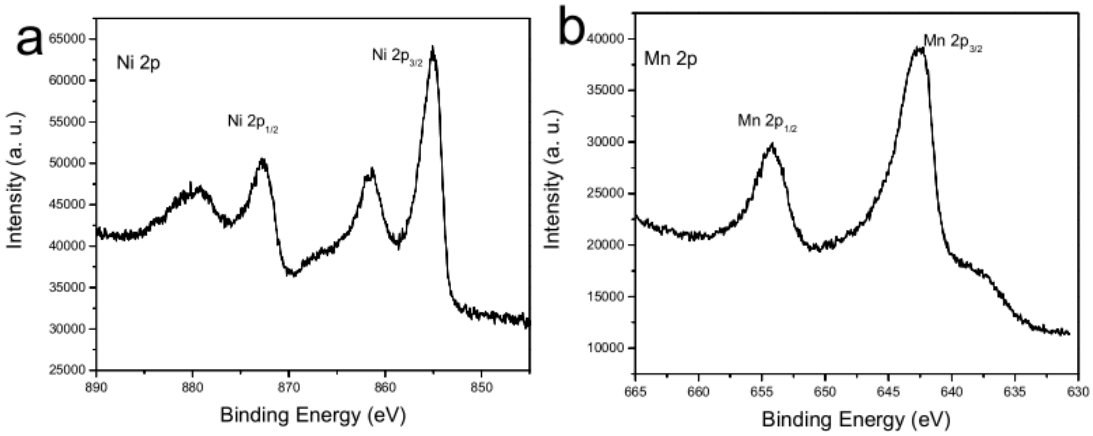

Figure 3. XPS spectra of the Li-rich $0.1Li_2MnO_3$ $0.9LiNi_{0.56}Mn_{0.44}O_2$ (a) Ni 2p, (b) Mn 2p.

Figure 4 presents the CV of the Li-rich $0.1Li_2MnO_3$ $0.9LiNi_{0.56}Mn_{0.44}O_2$ sample at a scan rate of 0.1 mV s^{-1} in a voltage range of 2.5-4.8 V. The anodic peak at about 4.2 V is assigned promarily to the oxidation of Ni^{2+} and Ni^{3+} to Ni^{4+}, meanwhile, the another anodic peak around 4.8 V is principally associated with the extraction of Li^+ from Li_2MnO_3 component accompanying with the extraction of oxygen and structural rearrangement [37-39].

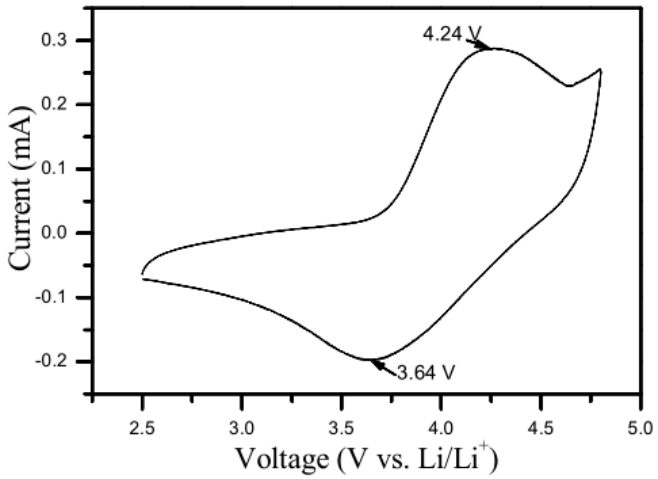

Figure 4. CV curve of the Li-rich $0.1Li_2MnO_3$ $0.9LiNi_{0.56}Mn_{0.44}O_2$ (scan rate: 0.1 mV s^{-1}, potential range: 2.5-4.8 V).

Figure 5a dispalys the initial and subsequent charge/discharge curves of the Li-rich $0.1Li_2MnO_3$ $0.9LiNi_{0.56}Mn_{0.44}O_2$ sample at a rate of 20 mA g^{-1} within a potential range from 2.5-4.8 V. Apparently, all the curves have similar profiles except the initial charge/discharge curve, which exhibits a smooth voltage slope below 4.5 V and a flat plateau above 4.5 V. The slope curve below 4.5 V can be attributed to the lithium ion extraction from the layered $LiMO_2$ framwork and the oxidation of the Ni^{2+}/Ni^{4+} and Ni^{3+}/Ni^{4+}, while the plateau above 4.5 V was in accordance with the irreversible removal of Li_2O from the Li_2MnO_3 component, which commonly leads to larger initial irreversible capacity fading and lower coulombic efficiency [40]. Compared to the Li-rich Li-Ni-Mn-Co-O layered cathode materials [41-43], the cobalt-free Li-rich $0.1Li_2MnO_3$ $0.9LiNi_{0.56}Mn_{0.44}O_2$ layered oxide demonstrates only smaller initial charge and discharge capacity fading, indicating that the Li-rich Li-Ni-Mn-O layers inhibit the electrochemical inactivation of the cathode material. However, there is no plateau at about 4.5 V observed in the 2nd and subsequent charging process, indicating that the release of oxygen and electrolyte side reaction only occurred in the initial charging process. In addition, the discharge voltage lower than 3.5 V has not been observed in the 2nd and subsequent discharge process,

demonstrating that the tetravalent manganese ions are not reduced to a trivalent state by the irreversible oxygen release that occurs during the initial charging proceess [44]. Besides, the cobalt-free Li-rich $0.1Li_2MnO_3$ $0.9LiNi_{0.56}Mn_{0.44}O_2$ sample displays a significantly high initial reversible capacity of 264.9 mAh g^{-1} and a high coulombic efficiency of 94.3%, which is obviously enhanced in comparison with the Li-rich Li-Ni-Mn-Co-O layered cathode materials [41-43]. When charge-discharged over 2.5-4.8 V for 51 cycles, the cobalt-free Li-rich $0.1Li_2MnO_3$ $0.9LiNi_{0.56}Mn_{0.44}O_2$ sample shows a capacity of 240.7 mAh g^{-1} and 90.8% of initial capacity retention after 51 cycles in figure 5b, exhibiting an eminent structural reversibility and good cycle performance.

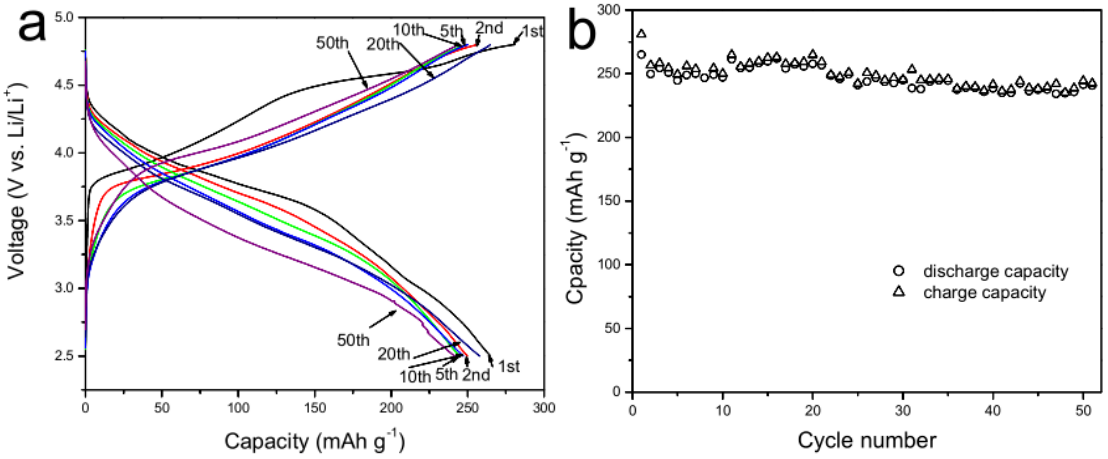

Figure 5. The initial and subsequent charge and discharge curves of Li-rich $0.1Li_2MnO_3$ $0.9LiNi_{0.56}Mn_{0.44}O_2$ (a) in the voltage from 2.5 to 4.8 V at a rate of 20 mA g^{-1}, and charge and discharge capacity as a function of cycle number (b).

Figure 6a displays the initial charge and discharge curves of Li-rich $0.1Li_2MnO_3$ $0.9LiNi_{0.56}Mn_{0.44}O_2$ sample in the voltage from 2.5 to 4.8 V at different current density of 50, 160, 320 and 640 mA g^{-1}, respectively. It can be seen from the curves that there is an desrease at the plateau of above 4.5 V in the initial charging process with the increasing of the current density. This phenomenon does not mean that the amounts of the release of oxygen and electrolyte side reaction during the initial charging process are decreasing with the increase of the current density, but the rates of oxygen release increase with the inrease of current density, while the speed of lithium extraction adding. Therefore, these phenomenons are embodied decreasing the plateau of above 4.5 V in the initial charge curves. Besides, the cycling performance of Li-rich $0.1Li_2MnO_3$ $0.9LiNi_{0.56}Mn_{0.44}O_2$ sample at different current density of 50, 160, 320 and 640 mA g^{-1} are shown in figure 7b with the initial discharge capacity are 263, 173, 137 and 57 mAh g^{-1}, respectively. After 51 cycles, the capacity decreased to 213, 117, 98 and 42 mAh g^{-1}, with capacity retentions of 81.9 %, 67.6 %, 71.5% and 73.7 %, respectively. Figure 7c shows that the capacity of the Li-rich layered sample is stable at each current density. Upon increasing the current density, the layered sample shows gradual reduced storage capacity was not due to an irreversible structural change, but to a diffusion-limited end-of-life polarization resulting from limited electronic conductivity and slow lithium-ion diffusion either across the electrolyte-electrode interface or within the bulk of the microspheres [15]. Therefore, the excellent electrochemical properties of $0.1Li_2MnO_3$ $0.9LiNi_{0.56}Mn_{0.44}O_2$ sample could be related to the specific morphology, which can maintain homogeneous intercalation reversibility for Li^+ and efficient contact areas between the cathode material and electrolyte during the cycles. Simultaneously, the micro-matrix assembled with nanoscale primary particles can consolidate the integrity of the host structure and shorten the transfer distance of Li^+. Accordingly, the abundant pore structures not only accelerate the penetration of electrolyte but also suppress the volume changes upon repeated Li^+ insertion/extraction procedures, thus improving the rate capacity and keeping the structure stability of Li-rich layered oxides.

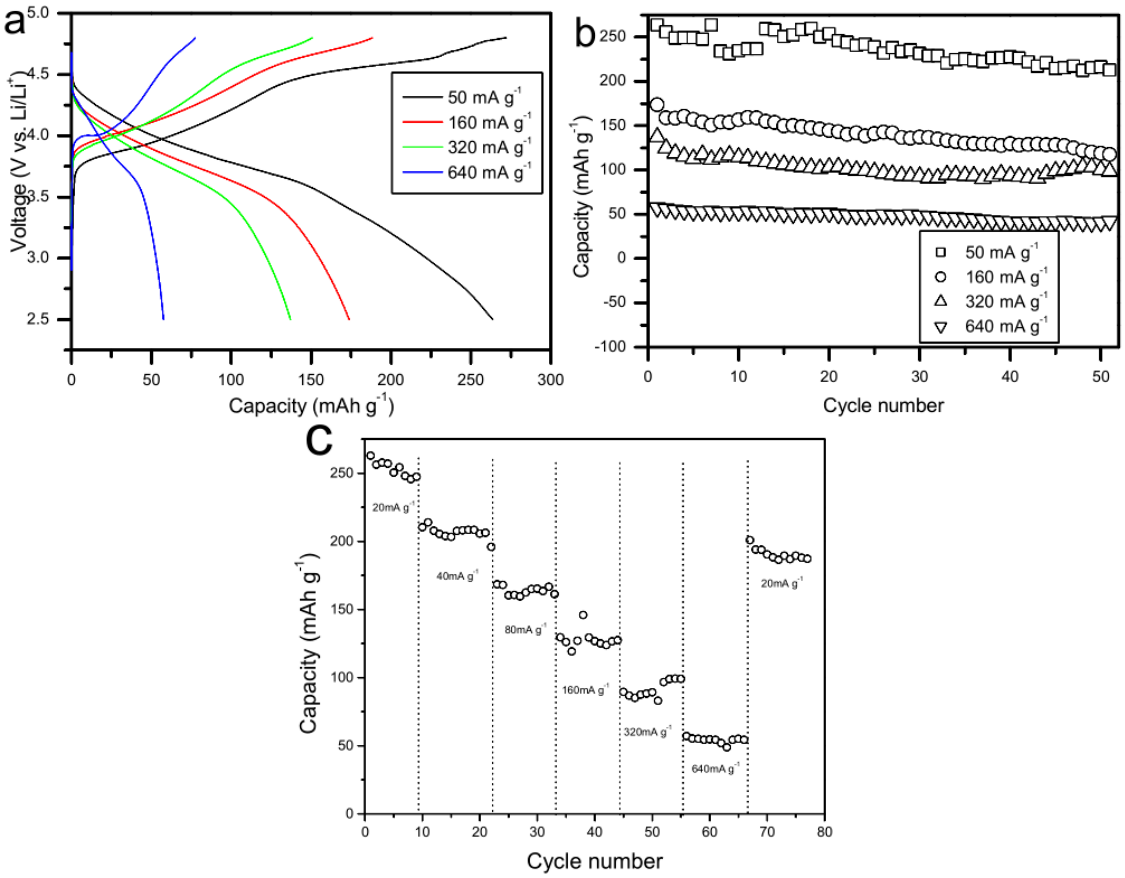

Figure 6. (a) The initial charge and discharge curves, (b) cycling performances and (c) discharge capacity of the Li-rich $0.1Li_2MnO_3$ $0.9LiNi_{0.56}Mn_{0.44}O_2$ in the voltage from 2.5 to 4.8 V at different current density.

4. Conclusions

In conclusion, cobalt-free Li-rich $0.1Li_2MnO_3$ $0.9LiNi_{0.56}Mn_{0.44}O_2$ as cathode material for lithium-ion batteries have been prepared by a coprecipitation approach followed by high temperature calcinations. Characterization results show that the sample possesses typical **α**-$NaFeO_2$ layered structure with the weak reflection of $LiMnO_6$, low degree of cation mixing, with morphology of microspheres with porous surface. The cobalt-free Li-rich $0.1Li_2MnO_3$ $0.9LiNi_{0.56}Mn_{0.44}O_2$ exhibits the high discharge capacity of 240.7 mAh g^{-1} after 51 cycles in the potential range of 2.5-4.8 V at a current of 20 mA g^{-1} with the release of oxygen and electrolyte side reaction only occurring in the initial charging process. And the obtained cobalt-free Li-rich $0.1Li_2MnO_3$ $0.9LiNi_{0.56}Mn_{0.44}O_2$ delivers good cycling stability and rate capability, which can be a promising cathode candidate for high energy density lithium-ion batteries.

5. Acknowledgement

The research was supported by the science and technology plan projects of Baoji (16RKX1-18), and the Natural Science Foundation of China (51702006).

6. References

[1] K. Bourzac, Batteries: 4 big questions, Nature 526 (2015) S105.
[2] H. Tavassol, E. M. C. Jones, N. R. Sottos, A. A. Gewirth, Electrochemical stiffness in lithium-ion batteries, Nature Mater. 15 (2016) 1182–1187.
[3] Y.-K. Sun, S.-T. Myung, B.- C. Park, J. Prakash, I. Belharouak, K. Amine, High-energy cathode material for long-life and safe lithium batteries, Nature Mater. 8 (2009) 320 - 324.

[4] P. K. Nayak, E. M. Erickson, F. Schipper, T. R. Penki, N. Munichandraiah, P. Adelhelm, H. Sclar, F. Amalraj, B. Markovsky, D. Aurbach, Review on Challenges and Recent Advances in the Electrochemical Performance of High Capacity Li- and Mn-Rich Cathode Materials for Li-Ion Batteries, Adv. Energy Mater., 16 (2017) 1702397 (1-16).
[5] F. Wu, H. Lu, Y. Su, N. Li, L.g Bao, S. Chen, Preparation and electrochemical performance of Li-rich layered cathode material, Li $[Ni_{0.2}Li_{0.2}Mn_{0.6}]$ O_2, for lithium-ion batteries, J. Applied Electrochem. 40 (2010) 783-789.
[6] H. Deng, I. Belharouak, R. E. Cook, H. Wu, Y.-K. Sun, K. Amine, Nanostructured Lithium Nickel Manganese Oxides for Lithium-Ion Batteries, J. Electrochem. Soc. 157 (2010) A447-A452.
[7] A. Boulineau, L. Simonin, J.-F. Colin, C. Bourbon, S. Patoux, First Evidence of Manganese–Nickel Segregation and Densification upon Cycling in Li-Rich Layered Oxides for Lithium Batteries, Nano Lett. 13 (2013) 3857-3863.
[8] L. Simonin, J.-F. Colin, V. Ranieri, E. Canévet, J.-F. Martin, C. Bourbon, C. Baehtz, P. Strobel, L. Daniel, S. Patoux, In situ investigations of a Li-rich Mn–Ni layered oxide for Li-ion batteries, J. Mater. Chem. 22 (2012) 11316-11322.
[9] M. Chen, E. Zhao, D. Chen, M. Wu, S. Han, Q. Huang, L. Yang, X. Xiao, and Z.Hu, Decreasing Li/Ni Disorder and Improving the Electrochemical Performances of Ni-Rich $LiNi_{0.8}Co_{0.1}Mn_{0.1}O_2$ by Ca Doping, Inorg. Chem. 56 (2017) 8355–8362.
[10] T. Tang, H.-L. Zhang, Synthesis and electrochemical performance of lithium-rich cathode material Li $[Li_{0.2}Ni_{0.15}Mn_{0.55}Co_{0.1-x}Al_x]$ O_2, Electrochim. Acta, 191 (2016) 263-269.
[11] L. Li, B.H. Song, Y.L. Chang, H. Xia, J.R. Yang, K.S. Lee, L. Lu, Retarded phase transition by fluorine doping in Li-rich layered $Li_{1.2}Mn_{0.54}Ni_{0.13}Co_{0.13}O_2$ cathode material, J. Power Sources 283 (2015) 162-170.
[12] J. H. Song, A. Kapylou, H. S. Choi, B. Y. Yu, E. Matulevich, S. H. Kang, Suppression of irreversible capacity loss in Li-rich layered oxide by fluorine doping, J. Power Sources 313 (2016) 65-72.
[13] S. H. Lee, J.-S. Moon, M.-S. Lee, T.-H. Yu, H.n Kim, B. M. Park, Enhancing phase stability and kinetics of lithium-rich layered oxide for an ultra-high performing cathode in Li-ion batteries, J. Power Sources 281 (2015) 77-84.
[14] T. Zhao, N. Zhou, X. Zhang, Q. Xue, Y. Wang, M. Yang, L. Li, and R. Chen, Structure Evolution from Layered to Spinel during Synthetic Control and Cycling Process of Fe-Containing Li-Rich Cathode Materials for Lithium-Ion Batteries, ACS Omega 2 (2017) 5601–5610.
[15] G. Kobayashi, Y. Irii, F. Matsumoto, A. Ito, Y. Ohsawa, S. Yamamoto, Y. Cui, J.-Y. Son, Y. Sato, Improving cycling performance of Li-rich layered cathode materials through combination of Al_2O_3-based surface modification and stepwise precycling, J. Power Sources 303 (2016) 250-256.
[16] F. Wu, J. Liu, L. Li, X. Zhang, R. Luo, Y. Ye, and R. Chen, Surface Modification of Li-Rich Cathode Materials for Lithium-Ion Batteries with a PEDOT:PSS Conducting Polymer, ACS Appl. Mater. Interfaces 8 (2016) 23095–23104.
[17] S. Zhang, H. Gu, T. Tang, W. Du, M. Gao, Y. Liu, D. Jian, and H. Pan, In Situ Encapsulation of the Nanoscale Er_2O_3 Phase To Drastically Suppress Voltage Fading and Capacity Degradation of a Li- and Mn-Rich Layered Oxide Cathode for Lithium Ion Batteries, ACS Appl. Mater. Interfaces 9 (2017) 33863–33875.
[18] F. Zheng ,C. Yang, X. Xiong, J. Xiong, R. Hu, Y. Chen, M. Liu, Nanoscale Surface Modification of Lithium-Rich Layered-Oxide Composite Cathodes for Suppressing Voltage Fade, Angew. Chem.-Int. Edit. 54 (2015) 13058–13062
[19] Y.-P. Deng, Z.-W. Yin, Z.-G. Wu, S.-J. Zhang, F. Fu, T. Zhang, J.-T. Li, L. Huang, and S.-G. Sun, Layered/Spinel Heterostructured and Hierarchical Micro/Nanostructured Li-Rich Cathode Materials with Enhanced Electrochemical Properties for Li-Ion Batteries, ACS Appl. Mater. Interfaces 9 (2017) 21065–21070.
[20] L. Yi, Z. Liu, R. Yu, C. Zhao, H. Peng, M. Liu, B. Wu, M. Chen, and X. Wang, Li-Rich Layered/Spinel Heterostructured Special Morphology Cathode Material with High Rate Capability for Li-Ion Batteries, ACS Sustainable Chem. Eng. 5 (2017) 11005–11015.

[21] K. Wu, G. Jia, X. Shangguan, G. Yang, Z. Zhu, Z. Peng, Q. Zhuge, F. Li, X. Cui and S. Liu, Improving the Electrochemical Performance of Ni-rich $LiNi_{0.8}Co_{0.1}Mn_{0.1}O_2$ by Enlarging the Li Layer Spacing, Energy Technology. (2018) DOI: 10.1002/ente.201700939.
[22] Y. Zou, X. Yang, C. Lv, T. Liu, Y. Xia, L. Shang, G. I. N. Waterhouse, D. Yang and T. Zhang, Multishelled Ni-Rich $Li(Ni_xCo_yMn_z)O_2$ Hollow Fibers with Low Cation Mixing as High-Performance Cathode Materials for Li-Ion Batteries, Adv.Sci. 4 (2017), 1600262 (1-8).
[23] A. Ito, D. Li, Y. Sato, M. Arao, M. Watanabe, M. Hatano, H. Horie, Y. Ohsawa, Cyclic deterioration and its improvement for Li-rich layered cathode material $Li[Ni_{0.17}Li_{0.2}Co_{0.07}Mn_{0.56}]O_2$, J. Power Sources 195 (2010) 567-573.
[24] M. M. Thackeray, S.-H. Kang, C. S. Johnson, J. T. Vaughey, R. Benedek, S. A. Hackney, Li_2MnO_3-stabilized $LiMO_2$ (M = Mn, Ni, Co) electrodes for lithium-ion batteries, J. Mater. Chem. 17 (2007) 3112–3125.
[25] Z. H. Lu, D. D. MacNeil, J. R. Dahn, Layered Cathode Materials $Li[Ni_xLi_{(1/3-2x/3)}Mn_{(2/3-x/3)}]O_2$ for Lithium-Ion Batteries, Electrochem. Solid State Lett. 4 (2001) A191–A194.
[26] A. R. Armstrong, M. Holzapfel, P. Novak, C.S. Johnson, S.-H. Kang, M.M. Thackeray, P.G. Bruce, Demonstrating Oxygen Loss and Associated Structural Reorganization in the Lithium Battery Cathode $Li[Ni_{0.2}Li_{0.2}Mn_{0.6}]O_2$, J. Am. Chem. Soc. 128 (2006) 8694–8698.
[27] B. Song, H. Liu, Z. Liu, P. Xiao, M. O. Lai, L. Lu, High Rate Capability Caused by Surface Cubic Spinels in Li-rich Layer-Structured Cathodes for Li-Ion Batteries, Sci. Rep. 3 (2013) 3094.
[28] Y. Zhang, Y. Li, X. Niu, D. Wang, D. Zhou, X. Wang, C. Gu, J. Tu, A Peanut-Like Hierarchical Micro/Nano-$Li_{1.2}Mn_{0.54}Ni_{0.18}Co_{0.08}O_2$ Cathode Material for Lithium-Ion Batteries with Enhanced Electrochemical Performance, J. Mater. Chem. A 3 (2015) 14291-14297.
[29] G. Wang, X. Wang, L. Yi, R. Yu, M. Liu, X. Yang, Preparation and Performance of $0.5Li_2MnO_3$ $0.5LiNi_{1/3}Co_{1/3}Mn_{1/3}O_2$ with a Fusiform Porous Micro-Nano Structure, J. Mater. Chem. A 4 (2016) 15929-15939.
[30] C. Zhao, X. Wang, R. Liu, X. Liu, Q. Shen, Oxalate Precursor Preparation of $Li_{1.2}Ni_{0.13}Co_{0.13}Mn_{0.54}O_2$ for Lithium Ion Battery Positive Electrode, Ionics 20 (2014) 645-652.
[31] S. J. R. Prabakar, S. C. Han, S. P. Singh, D. K. Lee, K.-S. Sohn, M. Pyo, W-doped $LiW_xNi_{0.5}Mn_{1.5-x}O_4$ cathodes for the improvement of high rate performances in Li ion batteries, J. Power Sources 209 (2012) 57-64.
[32] C. Yu, G. S. Li, X. F. Guan, J. Zheng, L. P. Li, T. W. Chen, Composites Li_2MnO_3 ŁiMn$_{1/3}$Ni$_{1/3}$Co$_{1/3}$O$_2$: Optimized synthesis and applications as advanced high-voltage cathode for batteries working at elevated temperatures, Electrochim. Acta 81 (2012) 283-291.
[33] M. Oishi, T. Fujimoto, Y. Takanashi, Y. Orikasa, A. Kawamura, T. Ina, H. Yamashige, D. Takamatsu, K. Sato, H. Murayama, H. Tanida, H. Arai, H. Ishii, C. Yogi, I. Watanabe, T. Ohta, A. Mineshige, Y. Uchimoto, Z. Ogumi, Charge compensation mechanisms in $Li_{1.16}Ni_{0.15}Co_{0.19}Mn_{0.50}O_2$ positive electrode material for Li-ion batteries analyzed bu a combination of hard and X-ray absorption near edge structure, J. Power Sources 222 (2013) 45-51.
[34] K. Amine, H. Tukamoto, H. Yasuda, Y. Fujita, A new three-volt spinel $Li_{1-x}Mn_{1.5}Ni_{0.5}O_4$ for secondary lithium batteries, J. Electrochem. Soc. 143 (1996) 1607-1613.
[35] C. Lu, S. Yang, H. Wu, Y. Zhang, X. Yang, T. Liang, Enhanced electrochemical performance of Li-rich $Li_{1.2}Mn_{0.52}Co_{0.08}Ni_{0.2}O_2$ cathode materials for Li-ion batteries by vanadium doping, Electrochim. Acta 209 (2016) 448-455.
[36] T. Yang, N. Zhang, Y. Lang, K. Sun, Enhanced rate performance of carbon-coated $LiNi_{0.5}Mn_{1.5}O_4$ cathode material for lithium ion batteries, Electochim. Acta 56 (2011) 4058-4064.
[37] A. R. Armstrong, M. Holzapfel, P. Novak, C. S. Johnson, S. H. Kang, M. M. Thackeray, P. G. Bruce, Demonstrating Oxygen Loss and Associated Structural Reorganization in the Lithium Battery Cathode $Li[Ni_{0.2}Li_{0.2}Mn_{0.6}]O_2$, J. Am. Chem. Soc. 128 (2006) 8694-8698.
[38] Y. Li, Y. Bai, C. Wu, J. Qian, G. Chen, L. Liu, H. Wang, X. Zhou, F. Wu, Three-Dimensional Fusiform Hierarchical Micro/Nano $Li_{1.2}Ni_{0.2}Mn_{0.6}O_2$ with a Preferred Orientation (110) Plane as

a High Energy Cathode Material for Lithium-Ion Batteries, J. Mater. Chem. A 4 (2016) 5942-5951.

[39] G. Wang, X. Wang, L. Yi, L. Wang, R. Yu, M. Liu, D. Wang, Q. Ren, X. Yang, The Effects of $LiTi_2(PO_4)_3$ Modification on the Performance of Spherical $Li_{1.5}Ni_{0.25}Mn_{0.75}O_{2+\delta}$ Cathode Material, RSC Adv. 6 (2016) 46325-46335.

[40] J. Yang, F. Cheng, X. Zhang, H. Gao, Z. Tao, J. Chen, Porous $0.2Li_2MnO_3$ $0.8LiNi_{0.5}Mn_{0.5}O_2$ Nanorods as Cathode Materials for Lithium-Ion Batteries, J. Mater. Chem. A 2 (2014) 1636-1640.

[41] B. Qiu, C. Yin, Y. Xia, Z. Liu, Synthesis of Three-Dimensional Nanoporous Li-Rich Layered Cathode Oxides for High Volumetric and Power Energy Density Lithium-Ion Batteries, ACS Appl. Mater. Interfaces 9 (2017) 3661−3666.

[42] P. K. Nayak, J. Grinblat, M. Levi, E. Levi, S. Kim, J. W. Choi, D. Aurbach, Al Doping for Mitigating the Capacity Fading and Voltage Decay of Layered Li and Mn-Rich Cathodes for Li-Ion Batteries, Adv. Energy Mater. 6 (2016) 1502398.

[43] Y. Su, G. Chen, L. Chen, W. Li, Q. Zhang, Z. Yang, Y. Lu, L. Bao, J. Tan, R. Chen, S. Chen, F. Wu, Exposing the {010} planes by oriented self-assembling with nanosheets to improve the electrochemical performances of Ni-rich $Li[Ni_{0.8}Co_{0.1}Mn_{0.1}]O_2$ microspheres, ACS Appl. Mater. Interfaces (2018) DOI: 10.1021/acsami.7b18933.

[44] D. Liu, J. Han, J. B. Goodenough, Structure, morphology, and cathode performance of $Li_{1-x}[Ni_{0.5}Mn_{1.5}]O_4$ prepared by coprecipitation with oxalic acid, J. Power Sources 195 (2010) 2918-2923.